Charge–Discharge Property of Si and SiO_x Nanoparticles Produced in Regulated Carbon Nanospace

Hikaru Tabuchi, Tsuyoshi Nakamura, Koki Urita, and Isamu Moriguchi*
Graduate School of Engineering, Nagasaki University, 1-14 Bunkyo-machi, Nagasaki 852-8521

(E-mail: mrgch@nagasaki-u.ac.jp)

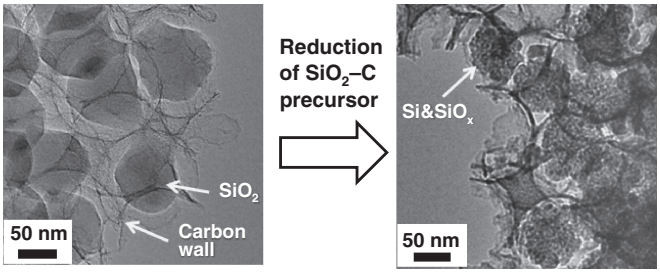

The present work developed Si and SiO_x nanoparticle-embedded nanoporous carbons with tunable interstitial nanospace and revealed that dispersive loading of Si and SiO_x nanoparticles in carbon nanospace is necessary to enhance the charge–discharge performance in addition to providing the interstitial nanospace as a buffer space for the volume change with Si–Li reactions.

REPRINTED FROM

Chemistry Letters

Vol.44 No.1 2015 p.23–25

CMLTAG
January 5, 2015

The Chemical Society of Japan

Received: September 14, 2014 | Accepted: October 2, 2014 | Web Released: October 8, 2014 CL-140862

Charge–Discharge Property of Si and SiO_x Nanoparticles Produced in Regulated Carbon Nanospace

Hikaru Tabuchi, Tsuyoshi Nakamura, Koki Urita, and Isamu Moriguchi*
Graduate School of Engineering, Nagasaki University, 1-14 Bunkyo-machi, Nagasaki 852-8521

(E-mail: mrgch@nagasaki-u.ac.jp)

Si and SiO_x nanoparticle-embedded nanoporous carbons were successfully synthesized by reducing a SiO_2 opal–carbon composite precursor with Mg, and their interstitial nanospace in carbon pores was tunable by partly etching the SiO_2 particles in the precursor. It was revealed that dispersive loading of Si and SiO_x nanoparticles in carbon nanospace is necessary to enhance the charge–discharge performance in addition to providing the interstitial nanospace as a buffer space for the volume change associated with Si–Li reactions.

Lithium-ion secondary batteries (LIBs) are attractive power storage devices, but they need to be further improved for power-grid applications as well as power sources of electric and/or hybrid electric vehicles. Silicon is expected to be a candidate negative electrode material for high-energy LIBs because of the extremely high theoretical capacity (ca. 4200 mA h g^{-1}) based on Si–Li alloying and dealloying reactions. However, severe capacity fading with charge–discharge cycling is generally observed because of cracking and crumbling in Si-integrated electrodes, which is caused by the large volume change between Li_xSi and original Si. To overcome the problem, Si dispersed in carbon matrices (Si–C composites) has been actively studied from the viewpoint of suppressing the loss of interparticle electronic contact with the pulverization of Si during Si–Li alloying and dealloying reactions.[1] Although the composites were effective in improving the cycle performance to some extent, recent research has focused on the development of nanostructured materials of Si and Si–C composite to yield superior performance. For example, Si nanomaterials with 3D nanoporous structure[2] and morphologies of nanotube[3,4] and hollow sphere[5] showed high capacities and good cycle performance. Si–C nanocomposite materials such as Si nanoparticles coated with carbon[6,7] and graphene sheet,[8,9] Si-loaded carbon nanofibers,[10,11] and nanoporous Si–C[12] were effective in enhancing the cycle performance. Providing both electronic conduction paths and buffer space for the large volume change between Li_xSi and Si is considered important to achieve high performance of Si-based negative electrodes. However, it is still unclear how to design and control the buffer space in carbon matrices to optimize the charge–discharge performance.

In the present study, a new process was developed for the production of Si and SiO_x nanoparticles in carbon nanopores while tuning the interstitial nanospace between the nanoparticles and surrounding carbon wall. We also evaluated the effect of the nanospace and the nanoparticle-loading state on charge–discharge cyclability.

Si and SiO_x nanoparticles were produced in carbon nanopores by Mg thermal reduction of a SiO_2–carbon nanocomposite. The SiO_2–carbon composite was obtained by impregnating a mixture solution of phenol and aqueous formaldehyde into the interstitial space of a silica opal constructed with SiO_2 particles with the average diameter of 140 nm, followed by drying and heating at 1000 °C for 5 h as reported previously.[13,14] The SiO_2–carbon nanocomposite was grounded and sieved to a 80-mesh powder and then was dispersed in a 1.0 mol dm^{-3} solution of NaOH in ethanol/water (1/1 by volume) for 36 h under stirring. The filtrated powder was washed with pure water copiously and then was dried by heating at 200 °C in vacuo for 12 h. The sample is denoted as SiO_2–C(x), where x indicates the NaOH treatment (etching) time. The conversion of SiO_2 in SiO_2–C(x) into Si was carried out by heating a mixture of Mg powder and SiO_2–C(x) with the Mg/SiO_2 molar ratio of 2.0–2.5 at 590 °C for 4 h in an Ar atmosphere. The heated mixture was dispersed in a 0.5 mol dm^{-3} solution of HCl in ethanol/water (1/1 by volume) for 12 h and subsequently in 23 wt % HF solution in ethanol/water (1/1 by volume) to remove coproducts such as MgO, Mg_xSi, and SiO_2. The filtrated sample after the HCl as well as HF treatment was washed with pure water copiously and then was vacuum-dried at 120 °C for 2 h. Hereafter, the samples that have undergone the HCl treatment as well as both HCl and HF treatments are referred to as SiO_2–C(x)-Hall and SiO_2–C(x)-HF, respectively. Si nanoparticle powder with the average size of 20–30 nm was purchased from Nanostructured & Amorphous Materials, Inc. as a reference. A Si–porous carbon composite, which is denoted as Si–PC, was also prepared by vacuum impregnation of a Si nanoparticle-dispersed methanol solution into the silica opal-derived porous carbon, followed by filtration and drying at 100 °C for 12 h. The mixing condition for porous carbon/Si/methanol was 60 mg/60 mg/40 mL.

X-ray diffraction measurements confirmed that crystalline Si and MgO phases were produced in SiO_2–C(x) composites after heating with Mg, and the MgO phase disappeared after the HCl treatment (Figure S1 in Supporting Information). The carbon and SiO_2 contents in samples were determined by elementary and thermogravimetric analyses, respectively. Si derivatives produced in SiO_2–C(x)-HCl and SiO_2–C(x)-HF such as Si, SiO_x ($0 < x < 2$), and SiO_2 were analyzed by X-ray photoelectron spectroscopy (Figure S2 in Supporting Information). The specific surface area (S_a) and specific pore volume (V_p) of samples were determined from N_2 adsorption isotherms by using the Brunauer–Emmett–Teller (BET) method. The composition, S_a, and V_p of the samples are listed in Table 1. SiO_2–C(36) has smaller SiO_2 content and larger S_a and V_p than SiO_2–C(0), indicating that the NaOH treatment resulted in partial etching of SiO_2 in the composite. The decrease in SiO_2 particle size and production of interstitial space between SiO_2 particles and the carbon wall was observed by transmission electron microscopy (TEM), as shown in Figures 1a and 1b. After heating with Mg and subsequent HCl treatment, the spherical SiO_2 particles in SiO_2–C(x) changed to agglomerated nanoparticles composed of Si, SiO_x, and SiO_2 in the nanospace surrounded by the carbon

Table 1. Structural characteristics of samples

Samples	Content/wt %				S_a	V_p
	C	SiO_2	Si	SiO_x	/$m^2\,g^{-1}$	/$cm^3\,g^{-1}$
SiO_2–C(0)	3.1	96.9	—	—	37	0.17
SiO_2–C(36)	18.2	81.8	—	—	213	0.68
SiO_2–C(0)-HCl	6.9	52.7	3.3	16.2	181	0.53
SiO_2–C(36)-HCl	28.7	35.0	21.3	13.6	307	0.93
SiO_2–C(36)-HF	66.3	8.8	7.7	16.9	457	1.02
Si–PC	46.0	—	48.8	—	515	0.97

wall (Figures 1c and 1d). The carbon nanospace was closely packed with the nanoparticles for SiO_2–C(0)-HCl, but the interstitial space produced by etching with NaOH was maintained for SiO_2–C(36)-HCl. The content ratio of Si and SiO_x against SiO_2 for SiO_2–C(36)-HCl was higher than that for SiO_2–C(0)-HCl. This means that the reduction of SiO_2 with Mg was prompted by providing the interstitial space in the SiO_2–C(x) composite. The content of residual SiO_2 in SiO_2–C(36)-HCl decreased upon the HF treatment, and consequently S_a, V_p, and the content ratio of Si and SiO_x against SiO_2 increased for SiO_2–C(36)-HF in comparison with that for SiO_2–C(36)-HCl. Nanoparticles of Si and/or SiO_x, which were agglomerated for SiO_2–C(36)-HCl, were observed by TEM to be dispersed in carbon nanopores for SiO_2–C(36)-HF (Figure 1e). On the other hand, Si nanoparticles with the size of approximately 30 nm were deposited both in carbon nanopores and on the outer surface for Si–PC, as shown in Figure 1f.

Electrochemical charge–discharge measurements were carried out in a 1.0 mol dm^{-3} solution of $LiPF_6$ in ethylene carbonate/dimethyl carbonate (1/1 by volume) using a three-electrode cell equipped with Li counter and reference electrodes that were mixed with poly(vinylidene difluoride) (PVdF) with the weight ratio of 90:10, and the mixture was pressed on Ni mesh to be used as a working electrode. A working electrode composed of a mixture of Si nanoparticles and acetylene black (AB), denoted as Si–AB, was also prepared by mixing Si, AB, and PVdF with the weight ratio of 45:45:10. Charge–discharge curves were obtained by using the constant current (CC) mode at the current density of 100 mA g^{-1} in the potential range of 0.01–2.0 V vs. Li^+/Li after the initial discharging from open circuit voltage to 0.01 V. Figures 2a and 2b show the 1st charge–discharge curves and cycle performance, respectively. All samples exhibited a typical plateau below 0.3 V vs. Li/Li^+ in the discharge curves due to the Si–Li alloying reaction, which included the irreversible reaction for SEI formation. Si–PC and Si–AB showed smaller initial charge capacities based on the composite weight than SiO_2–C(36)-HCl having lower Si content in the electrode, and their capacities faded rapidly with cycling. The cycle performance of Si–PC and Si–AB was inferior to that of SiO_2–C(36)-HCl and SiO_2–C(36)-HF. These results indicate that the confinement of Si nanoparticles in the carbon nanospace enhances the charge–discharge performance. Among SiO_2–C(x)-HCl and SiO_2–C(36)-HF samples, the initial charge capacity tended to increase with the increase of the Si and SiO_x contents, but this was not the case after the cycling (Figure 3a). The capacity retention of SiO_2–C(x)-HCl and SiO_2–C(36)-HF samples increased with increasing pore volume in composites, as shown in Figure 3b, rather than the Si and SiO_x contents. This means that introducing interstitial space near Si and SiO_x nanoparticles embedded in the carbon nanospace is effective in enhancing the reversibility of Si–Li alloying and dealloying reactions accompanied with a large volume change. However, the loading state of Si and SiO_x in carbon nanopores is also considered to affect the cyclability because the SiO_2–C(x)-HCl and SiO_2–C(36)-HF samples have enough pore volume even for four times volume expansion of $Li_{4.4}Si$ against Si. For example, the maximum expanded volume at $x = 0$ in SiO_x for SiO_2–

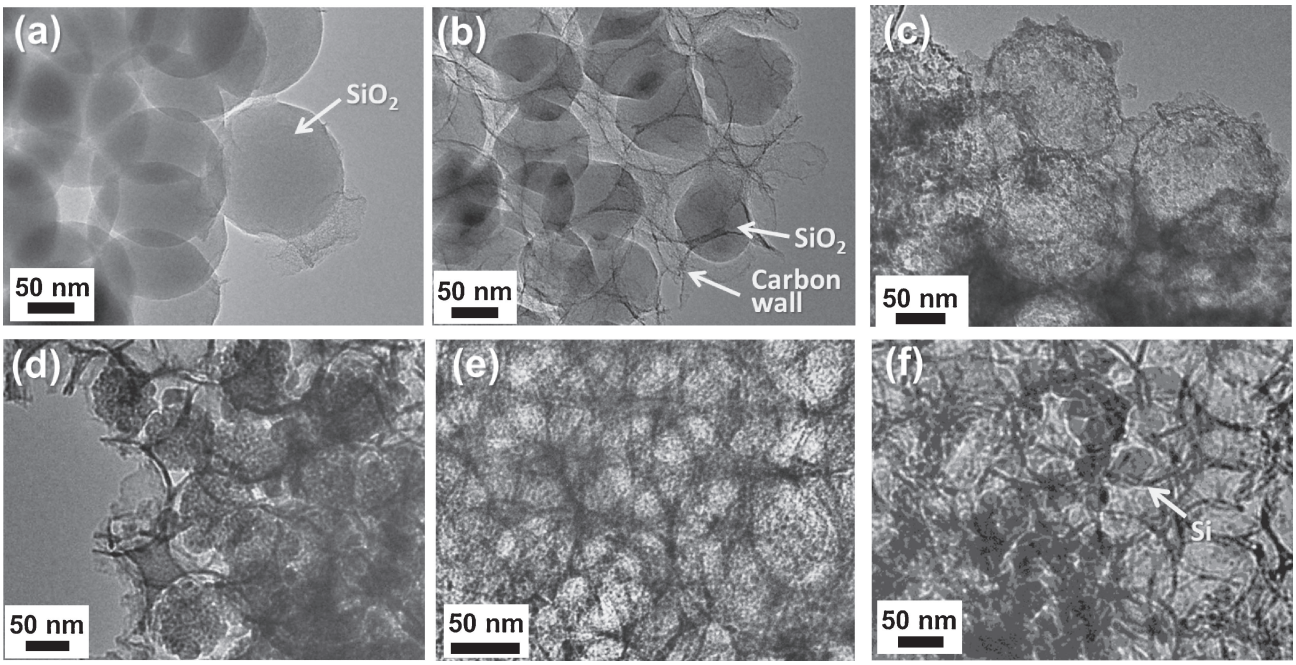

Figure 1. TEM images of (a) SiO_2–C(0), (b) SiO_2–C(36), (c) SiO_2–C(0)-HCl, (d) SiO_2–C(36)-HCl, (e) SiO_2–C(36)-HF, and (f) Si–PC.

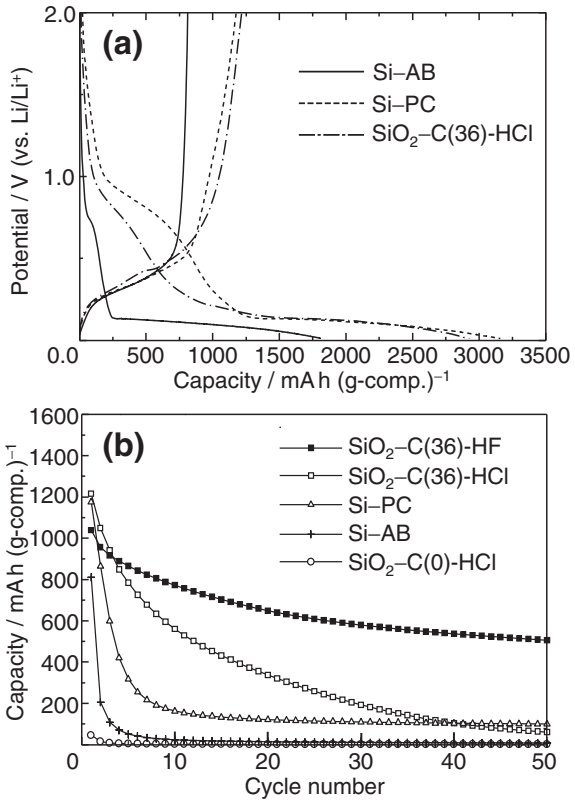

Figure 2. (a) Initial charge–discharge curves of SiO_2–AB, Si–PC, and SiO_2–C(36)-HCl and (b) cycle performance of Si–AB, Si–PC, and SiO_2–C(x) samples.

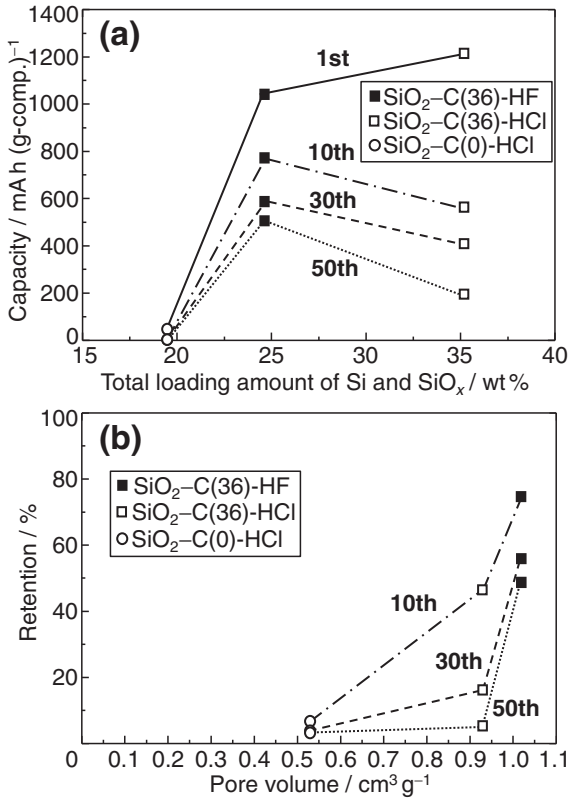

Figure 3. (a) Dependence of charge capacity of SiO_2–C(x) samples on Si and SiO_x loading amount and (b) dependence of the capacity retention on pore volume.

C(36)-HCl was calculated to be 0.61 cm^3 (g-comp.)$^{-1}$, which is smaller than the measured V_p. A large amount of inactive SiO_2 remaining in the agglomerated nanoparticles will disturb the Si–Li alloying and dealloying reactions for SiO_2–C(x)-HCl samples, and the dispersive loading of Si and SiO_x nanoparticles in carbon nanopores will result in good cyclability for SiO_2–C(36)-HF.

In conclusion, Si and SiO_x nanoparticle-embedded nanoporous carbons, of which the interstitial nanospace is tunable, were developed in the present study. It was revealed that dispersion of Si and SiO_x nanoparticles in the carbon nanospace is necessary to enhance the charge–discharge performance in addition to providing the interstitial nanospace as a buffer space for the volume expansion associated with Si–Li alloying and dealloying reactions. Further investigation is now in progress to achieve higher performance of Si nanomaterials by tuning the size and volume of carbon nanospace as well as increasing the loading amount of highly dispersed Si nanocrystallites.

The study made use of instruments (elementary analysis, XRD, XPS, and TEM) in the Center for Instruments Analysis of Nagasaki University. This work was partly supported by the Advanced Low Carbon Technology Research and Development Program of Japan Science and Technology Agency (JST) and a Grant-in-Aid for Scientific Research from Ministry of Education, Culture, Sports, Science and Technology of Japan.

References

1 U. Kasavajjula, C. Wang, A. J. Appleby, *J. Power Sources* **2007**, *163*, 1003.
2 H. Kim, B. Han, J. Choo, J. Cho, *Angew. Chem., Int. Ed.* **2008**, *47*, 10151.
3 M.-H. Park, M. G. Kim, J. Joo, K. Kim, J. Kim, S. Ahn, Y. Cui, J. Cho, *Nano Lett.* **2009**, *9*, 3844.
4 Z. Wen, G. Lu, S. Mao, H. Kim, S. Cui, K. Yu, X. Huang, P. T. Hurley, O. Mao, J. Chen, *Electrochem. Commun.* **2013**, *29*, 67.
5 Y. Yao, M. T. McDowell, I. Ryu, H. Wu, N. Liu, L. Hu, W. D. Nix, Y. Cui, *Nano Lett.* **2011**, *11*, 2949.
6 S. Iwamura, H. Nishihara, T. Kyotani, *J. Power Sources* **2013**, *222*, 400.
7 G. Zhao, L. Zhang, Y. Meng, N. Zhang, K. Sun, *Mater. Lett.* **2013**, *96*, 170.
8 P. Wu, H. Wang, Y. Tang, Y. Zhou, T. Lu, *ACS Appl. Mater. Interfaces* **2014**, *6*, 3546.
9 Y. Du, G. Zhu, K. Wang, Y. Wang, C. Wang, Y. Xia, *Electrochem. Commun.* **2013**, *36*, 107.
10 H. Wu, G. Zheng, N. Liu, T. J. Carney, Y. Yang, Y. Cui, *Nano Lett.* **2012**, *12*, 904.
11 C. Zhang, R. Yu, T. Zhou, Z. Chen, H. Liu, Z. Guo, *Carbon* **2014**, *72*, 169.
12 H.-C. Tao, L.-Z. Fan, X. Qu, *Electrochim. Acta* **2012**, *71*, 194.
13 I. Moriguchi, F. Nakahara, H. Furukawa, H. Yamada, T. Kudo, *Electrochem. Solid-State Lett.* **2004**, *7*, A221.
14 H. Yamada, H. Nakamura, F. Nakahara, I. Moriguchi, T. Kudo, *J. Phys. Chem. C* **2007**, *111*, 227.

